NANO LETTERS

Caltech Library

Subscriber access provided by Caltech Library

Communication

Two-photon microscopy with a double-wavelength metasurface objective lens

Ehsan Arbabi, Jiaqi Li, Romanus J Hutchins, Seyedeh Mahsa Kamali, Amir Arbabi, Yu Horie, Pol Van Dorpe, Viviana Gradinaru, Daniel A Wagenaar, and Andrei Faraon

Nano Lett., **Just Accepted Manuscript** • Publication Date (Web): 17 Jul 2018

Downloaded from http://pubs.acs.org on July 17, 2018

Just Accepted

"Just Accepted" manuscripts have been peer-reviewed and accepted for publication. They are posted online prior to technical editing, formatting for publication and author proofing. The American Chemical Society provides "Just Accepted" as a service to the research community to expedite the dissemination of scientific material as soon as possible after acceptance. "Just Accepted" manuscripts appear in full in PDF format accompanied by an HTML abstract. "Just Accepted" manuscripts have been fully peer reviewed, but should not be considered the official version of record. They are citable by the Digital Object Identifier (DOI®). "Just Accepted" is an optional service offered to authors. Therefore, the "Just Accepted" Web site may not include all articles that will be published in the journal. After a manuscript is technically edited and formatted, it will be removed from the "Just Accepted" Web site and published as an ASAP article. Note that technical editing may introduce minor changes to the manuscript text and/or graphics which could affect content, and all legal disclaimers and ethical guidelines that apply to the journal pertain. ACS cannot be held responsible for errors or consequences arising from the use of information contained in these "Just Accepted" manuscripts.

ACS Publications

is published by the American Chemical Society. 1155 Sixteenth Street N.W., Washington, DC 20036

Published by American Chemical Society. Copyright © American Chemical Society. However, no copyright claim is made to original U.S. Government works, or works produced by employees of any Commonwealth realm Crown government in the course of their duties.

Two-photon microscopy with a double-wavelength metasurface objective lens

Ehsan Arbabi,[†] Jiaqi Li,[‡,¶] Romanus J. Hutchins,[§] Seyedeh Mahsa Kamali,[†] Amir Arbabi,[‖] Yu Horie,[†] Pol Van Dorpe,[‡,¶] Viviana Gradinaru,[⊥] Daniel A. Wagenaar,[⊥] and Andrei Faraon[*,†]

†*T. J. Watson Laboratory of Applied Physics and Kavli Nanoscience Institute, California Institute of Technology, 1200 E. California Blvd., Pasadena, CA 91125, USA*

‡*IMEC, Kapeldreef 75, B-3001 Leuven, Belgium*

¶*Department of Physics and Astronomy, KU Leuven, Celestijnenlaan 200 D, B-3001 Leuven, Belgium*

§*Department of Physics and Astronomy, University of Missouri Columbia, MO 65211*

‖*Department of Electrical and Computer Engineering, University of Massachusetts Amherst, 151 Holdsworth Way, Amherst, MA 01003, USA*

⊥*Division of Biology and Biological Engineering, California Institute of Technology, Pasadena, CA 91125, USA*

E-mail: faraon@caltech.edu

Abstract

Two-photon microscopy is a key imaging technique in life sciences due to its superior deep-tissue imaging capabilities. Light-weight and compact two-photon microscopes are of great interest because of their applications for *in vivo* deep brain imaging. Recently, dielectric metasurfaces have enabled a new category of small and light-weight optical elements, including objective lenses. Here we experimentally demonstrate two-photon microscopy using a

double-wavelength metasurface lens. It is specifically designed to focus 820-nm and 605-nm light, corresponding to the excitation and emission wavelengths of the measured fluorophors, to the same focal distance. The captured two-photon images are qualitatively comparable to the ones taken by a conventional objective lens. Our metasurface lens can enable ultra-compact two-photon microscopes with similar performance compared to current systems that are usually based on graded-index-lenses. In addition, further development of tunable metasurface lenses will enable fast axial scanning for volumetric imaging.

Keywords

Optical metasurface, flat optics, multi-wavelength lens, two-photon microscopy

Two-photon microscopy is widely used for deep tissue imaging in various areas of life sciences.[1–4] The method utilizes the lower scattering of near-IR light inside tissues, the higher transverse and lateral resolution, and the lower level of background fluorescence in two-photon excitation to form high-quality images hundreds of microns deep inside tissues.[3,4] Development of compact low-weight two-photon microscopes for *in vivo* imaging of brain activity has been of great interest in recent years.[5–10] For compactness and low-weight, most of these systems use graded index objective lenses with optical qualities inferior to the conventional refractive objectives.

Dielectric metasurfaces are a recent category of diffractive devices[11–13] that enable high-end optical elements like blazed gratings[14] and lenses[15–18] with high efficiencies, and with a thin and light-weight form factor. Metasurface devices integrated in thin layers[19,20] and on membranes[21] have milligram and microgram weights. Therefore, the weight of optics will not be a significant factor in the total weight of systems that employ metasurface optics. In addition, because of their novel capabilities[22–30] and manufacturability with conventional nano-fabrication techniques, metasurfaces have attracted a great deal of attention in the past few years, especially for imaging applications.[16,17,31] Fluorescence microscopy is an especially suitable area for meta-lenses as the fluorescence bandwidth is usually limited and predetermined. For instance, meta-lenses have recently been utilized to capture single-photon fluorescence images of diamond nano-crystals with

embedded silicon vacancy emitters where the effects of the finite fluorescence bandwidth were also studied.[18] Despite this, meta-lenses have not previously been employed for multi-photon fluorescence microscopy. The reason lies in the fact that they are conventionally designed for a single operation wavelength, while in fluorescence microscopy the focal positions at the excitation and emission wavelengths can be far apart due to the chromatic dispersion.[32–35] This can significantly reduce the excitation−collection efficiency in the system.

Here we propose and experimentally demonstrate two-photon fluorescence microscopy with a double-wavelength meta-lens (DW-ML) working as the objective lens. We use a birefringent dichroic dielectric metasurface platform to make the DW-ML that is designed to have the same focal distance at the excitation and emission wavelengths. We show that the DW-ML forms images that are qualitatively comparable to those taken with a refractive objective.

A simplified schematic of a two-photon microscope employing the DW-ML is shown in **Figure 1**a. "Long-wavelength" light from a high–peak power pulsed laser is collimated using the excitation optics, passes through a dichroic mirror and is focused inside the fluorescent sample using the DW-ML. At the focal point inside the fluorescent sample, "short-wavelength" photons are emitted upon the absorption of pairs of the long-wavelength photons. The DW-ML collimates the emitted fluorescent light which is then reflected off the dichroic mirror and detected by a photodetector through the collection optics. The DW-ML should be designed to focus both the excitation and emission wavelengths to the same distance. To achieve this goal, we use the birefringent dichroic meta-atom technique introduced before.[36] This is schematically shown in **Figure 1**b, where the DW-ML focuses horizontally polarized light at the long wavelength, and vertically polarized light at the short wavelength to the same focal distance, f.

Considering the available pulsed laser, the two-photon fluorescence microscopy setup, and the fluorescent molecules used, we chose the operation wavelengths to be 820 nm for excitation and 605 nm for emission (see Methods and Supporting Information Figure 1 for specifics of the measurements and the two-photon setup). Although materials such as TiO_2 might be suitable for a visible lens, the requirement of operation at the 820 nm near-IR wavelength necessitates a

high-index material such as silicon. To implement the DW-ML, we used polycrystalline silicon (p-Si) because it has a high-index and a low loss at the chosen operation wavelengths. Therefore, the metasurface is composed of p-Si nano-posts with a rectangular cross section, located at the vertices of a square lattice on a fused silica substrate. As schematically shown in **Figure 2**a, the structure is covered by an SU-8 polymer capping layer which provides mechanical robustness and protects the metasurface. The asymmetric rectangular cross-section of the nano-posts generates an effective structural birefringence, resulting in different transmission phases and amplitudes for x- and y-polarized light.[22] For proper choices of the nano-post height and lattice constant, the two phases along the two meta-atom axes can be controlled fully and independently. Therefore, the metasurface can be designed to perform two independent functions for the two orthogonal input polarizations. As we have previously shown, the same holds true even if the two orthogonal input polarizations have different wavelengths.[36] To provide the full 2π phase coverage at both wavelengths, the nano-post height was chosen to be 407 nm, and the lattice constant was set to 310 nm. The transmission amplitude and phase at both wavelengths are plotted in Supporting Information Figure 2 as a function of the widths of the nano-posts, w_x and w_y. As seen in these figures, with a proper choice of values for w_x and w_y (i.e., the in-plane dimensions of the nano-posts), a complete and independent phase coverage for the two polarizations is possible. Here, to find the nano-post that best provides a desired transmission phase, we have found the post sizes that minimize the weighted complex transmission errors for the two wavelengths (see Methods for more details). The chosen values for w_x and w_y are plotted in **Figure 2**b and **Figure 2**c versus the required phases at 820 nm and 605 nm.

Using the data in **Figure 2**b and **Figure 2**c, we designed the DW-ML with a diameter of 1.6 mm, and a numerical aperture (NA) of 0.5 (with a focal distance f $\sim$1.386 mm at 820 nm and 605 nm wavelengths). The 0.5 NA value is chosen to match that of the conventional objective lens used in the two-photon microscopy measurements. The lens is designed to focus light at both wavelengths to a tight spot without spherical aberrations. **Figure 3**a shows a scanning electron micrograph of a part of the fabricated DW-ML, before capping with the SU-8 layer. An optical

image of the finished device is shown in the inset of **Figure 3**a.

To characterize the DW-ML we used a measurement setup and procedure similar to the ones used in our previous report.[36] The lens was illuminated by a collimated laser beam, and the optical intensity distribution was captured in several planes parallel to the focal plane using a custom-built microscope (for details of the measurement procedure and setup see Methods and Supporting Information Figure 3). For characterization at the two wavelengths of interest we used two different light sources. An 822-nm laser diode was used as the excitation close to 820 nm, and a supercontinuum laser with a bandpass filter centered at 600 nm and a 10-nm full width at half maximum (FWHM) was used for the measurements close to 605 nm. The measured intensity distributions in the axial and focal planes are shown in **Figure 3**b and **Figure 3**c for the long and short wavelengths, respectively. The measured FWHMs in the focal plane are $\sim$0.93 μm and $\sim$0.68 μm at 822 nm and 600 nm. They are both close to their corresponding diffraction limited values of 0.85 μm and 0.62 μm. The DW-ML shows similar focal lengths at both wavelengths, with maximum intensities in the 1376 μm and 1380 μm planes at 822 nm and 600 nm, respectively. These values are close to the designed focal distance of $\sim$1386 μm. The long depth of focus and the elevated background in **Figure 3**c (for the 600-nm case) are caused by the considerable bandwidth of the source, and the diffractive chromatic dispersion of the metasurface lens.[35,37] Resulting from this chromatic dispersion, the difference between the focal distance at the side wavelengths of 595 nm and 605 nm (corresponding to the measurement bandwidth) is about 20 μm. This causes a significant portion of the total light power to be out of focus in each plane around the focal distance.

To measure the focusing efficiency, we used the setup shown in Supporting Information Figure 3b. To block the out-of-focus light, irises with $\sim$1.1 mm and $\sim$0.55 mm diameters (for 822 nm and 600 nm wavelengths, respectively) were placed in front of the photodetector in the image plane of the microscope. These correspond to 10-μm and 5-μm diameter apertures in the focal plane of the DW-ML, respectively. The focusing efficiencies, defined as the ratio of the power passing through the irises to the total incident power, were measured to be 61% and 27% at 822 nm and 600 nm, respectively. We should mention here that the 10-nm bandwidth of the 600-nm mea-

surement source resulted in the reduced measured efficiency through the enhanced depth of focus. The measured 27% "broadband" efficiency would correspond to a single-wavelength efficiency of ∼45% around 600 nm (see Supporting Information Section 1 for discussion and simulation results of the efficiency).

Finally, we characterized the operation of the DW-ML by using it as the objective in a two-photon microscope for imaging a fluorophore-coated polyethylene microsphere ∼90 μm in diameter (see Methods and Supporting Information Figure 1 for the microscope setup and details). **Figure 4**a shows a regular image of the microsphere captured with the conventional objective. The two-photon fluorescent images captured by the DW-ML and the conventional objective are shown in **Figure 4**b and **Figure 4**c, respectively.

The two images are qualitatively similar and almost all fluorescent clusters visible in **Figure 4**c can also be seen in **Figure 4**b. The exact focal planes in the two setups might be slightly different, and this may account for some of the discrepancies between the two images. In addition, there are some important differences that are innate to the use of the DW-ML. The collected photon count is about 15× lower for the DW-ML (the colormaps in **Figure 4**b and **Figure 4**c are in the same unit), while the excitation beam power for the DW-ML was ∼4.7× larger than for the conventional objective. A few factors contribute to the effectively lower efficiency of the DW-ML for the combined excitation–collection process. First, the excitation efficiency is lower because of the lower focusing efficiency of the DW-ML at 820 nm (∼61%). The collection efficiency is also limited by the 45% focusing efficiency close to 605 nm. For the unpolarized light emitted by the fluorophores, the collection efficiency is reduced to half of this value (∼22.5%). In addition, the chromatic dispersion of the DW-ML results in lower peak intensity in focus, which further reduces the two-photon fluorescence rate (see Supporting Information Section 1). Finally, the broad emission bandwidth of the fluorescence emission and the chromatic dispersion result in a lower collection efficiency, arising from the emitting molecule being out-of-focus because it has a wavelength other than 605 nm.

As discussed above, a few different factors determine the efficiency of two-photon microscopy

with the DW-ML. The single-wavelength focusing efficiencies at the excitation and emission spectra limit the collected power. As previously demonstrated,[36] using a high-index material with lower loss that has a larger index contrast with the capping layer results in higher focusing efficiencies. Moreover, employing more advanced optimization and design methods[38] can help realize higher focusing efficiencies. The diffractive chromatic dispersion of the DW-ML is another factor that decreases both the peak excitation intensity and the collection efficiency. We should note that the absolute value of chromatic dispersion (that is the absolute change in the focal distance for a given change in the operation wavelength) is linearly proportional to the focal distance. Therefore, a metasurface lens with the same NA but shorter focal distance has a wider operation bandwidth.[31] Moreover, the resolution and the collection efficiency only depend on the numerical aperture, not the absolute physical aperture size or the focal distance. Therefore, metasurface lenses are more suited for two-photon applications with shorter focal distances and smaller apertures (keeping the NA constant). Such characteristics are very attractive for miniaturized two-photon microscopes.[5–10] Moreover, the ability to independently control the function of the DW-ML at the two operation wavelengths allows for integration of the lens and the dichroic mirror in the same device. One method of implementing this is through separating the excitation and collection paths by designing the lens to collimate the emitted light in an off-axis direction. This can further reduce the total weight, size, complexity, and cost of the two-photon microscopy.

The DW-ML can be tuned using various techniques[19–21,39] to enable axial scanning for fast three-dimensional scanning. In addition, the singlet DW-ML has large off-axis geometric aberrations that limit its field of view significantly. To mitigate this problem, the corrected metasurface doublet scheme can be employed.[31,40]

Most fluorophores have higher emission efficiency if the two-photon excitation wavelength is slightly shorter than twice their emission spectrum peak. However, it is very challenging to design high efficiency DW-MLs where the two wavelengths are far apart using the birefringent meta-atoms utilized here. In such cases the meta-molecule method,[41] the spatial multiplexing technique,[42–44] or the topological optimization method[38] might be more promising.

Using the metasurface lens with high power pulsed laser sources can raise a few different issues. First, the high power might damage the metasurface. Here, we utilized the maximum available power of the pulsed laser ($\sim$1 W) for the two-photon imaging experiments and did not observe any detectable difference in the performance or appearance of the metasurface lens after exposure to the high-power laser. Nevertheless, further investigation of the maximum intensity and power that the metasurface lenses can withstand could be of interest. Another issue concerns the nonlinear processes that can be more significant with higher excitation intensities. For instance, it would be of value to study the effect of the input power on the level of two-photon absorption in the metasurface lens and how it might impact the overall device efficiency. Other nonlinear phenomena, such as second harmonic generation, can also be of interest as they have been observed in silicon-based metasurfaces.[45] We should note here, however, that in the two-photon imaging measurements performed in this manuscript we didn't observe an increased background level when using the metasurface lens [**Figure 4**b and **Figure 4**c].

In conclusion, we used the birefringent dichroic dielectric metasurface platform to realize a DW-ML. Using the DW-ML as the objective lens, we demonstrated two-photon microscopy with image qualities comparable to a conventional microscope objective. The effect of the large diffractive chromatic dispersion of the DW-ML was considered and discussed. As a proof of concept, this work demonstrates the capabilities and limitations of the dielectric metasurface platform in multi-photon microscopy. With the great interest in the development of more compact two-photon microscopes, we believe metasurfaces can play a significant role in this field.

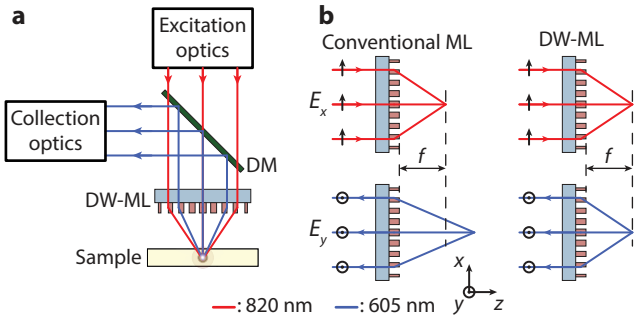

Figure 1: Schematic illustration of two-photon microscopy with a metasurface objective lens. (a) Schematics of a two-photon microscope employing a metasurface objective. A pulsed laser source is focused inside a sample using the excitation optics and a metasurface objective. The same metasurface lens along with the collection optics collects the light that is emitted by the sample through a two-photon fluorescence process. DM: Dichroic mirror; DW-ML: Double-wavelength metasurface lens. (b) Schematic illustration of a conventional metasurface lens focusing light with different wavelengths to distinct focal lengths, and the DW-ML designed to focus 820-nm x-polarized light and 605-nm y-polarized light to the same focal distance of f.

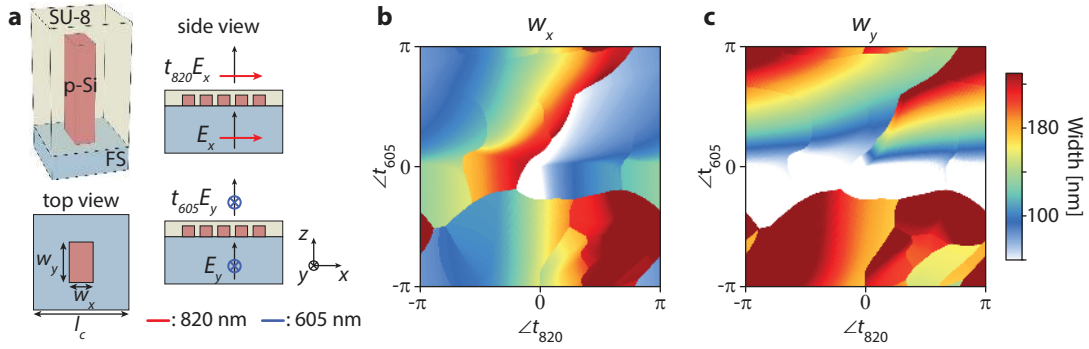

Figure 2: Meta-atom design. (a) Schematic illustration of the meta-atom, consisting of a p-Si nano-post with a rectangular cross-section sitting on a fused silica substrate and covered by an SU-8 layer. Top and side views of the nano-posts showing the dimensions and illumination conditions. Tuning the nano-post dimensions, w_x and w_y, allows for independent control of transmission phase of x-polarized light at 820 nm and y-polarized light at 605 nm. (b) The chosen values of w_x and (c) w_y versus the required phases for the two wavelengths. The nano-posts height is 407 nm and the lattice constant is 310 nm.

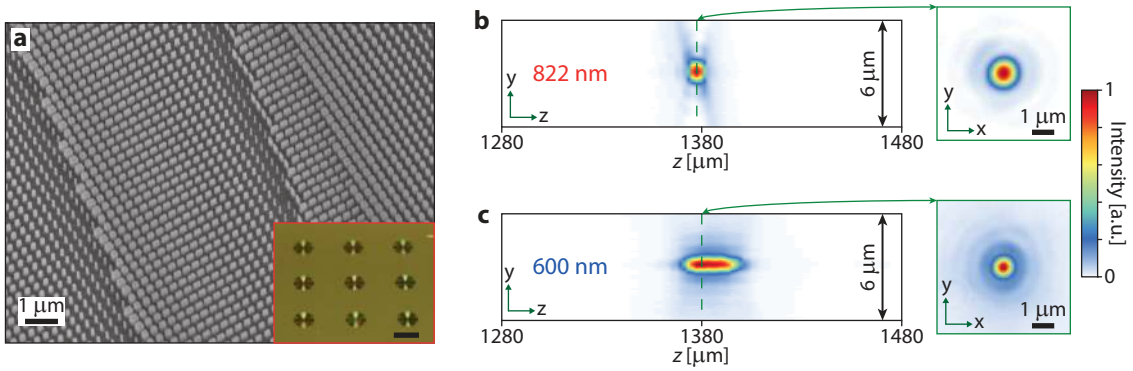

Figure 3: Characterization of the metasurface lens. (a) Scanning electron micrograph of a portion of the fabricated DW-ML. Inset: Optical image of a few fabricated lenses. Scale bar: 2 mm. (b) Measured light intensity in the axial (left) and focal (right) planes for x-polarized 822-nm illumination. (c) Same results as (b) for a y-polarized light source with a center wavelength of 600 nm and full width at half maximum of approximately 10 nm.

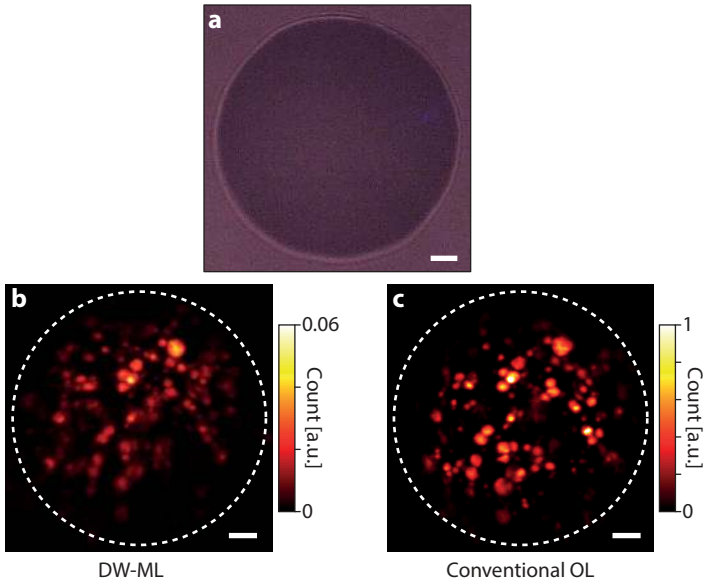

Figure 4: Two-photon microscopy with the DW-ML. (a) Regular microscope image of a fluorescent polyethylene microsphere. (b) Two-photon fluorescent microscope image of the microsphere in (a) captured using the DW-ML, and (c) captured using a conventional refractive objective. Scale bars: 10 μm.

Methods

Simulation. The transmission amplitude and phase of the nano-posts [Supporting Information Fig. 2] were acquired by simulating a uniform array of nano-posts on a square lattice using the rigorous coupled wave analysis technique.[46] The p-Si nano-posts were 407 nm tall, the lattice constant was 310 nm, and the refractive index of p-Si was 3.7231+0.0078i at 820 nm, and 3.9984+0.0282i at 605 nm. For the SU-8 layer, we used refractive index values of 1.58 and 1.595 at 820 nm and 605 nm, respectively. A normally incident plane-wave was used as the excitation. The simulations of Supporting Information Section 1 were performed using the calculated transmission mask of the lens, and the plane-wave expansion method.

Sample fabrication. A 458-nm thick layer of hydrogenated α-Si was deposited on a 1-mm-thick fused silica substrate using the plasma enhanced chemical vapor deposition technique. The layer was then annealed in a furnace to form the 407-nm-thick p-Si layer. The metasurface patterns were generated with electron-beam lithography in a positive electron-beam resist. An aluminum oxide layer was deposited on the generated pattern after development, and was used to reverse the pattern through lift-off. The patterned aluminum oxide layer was then used as a hard mask in the dry etching process of the p-Si layer. Finally, a $\sim$2-μm-thick layer of SU-8 was spin coated on the metasurface, and a gold aperture was deposited around the lens to reduce the background light.

Measurement procedure. The setup in Supporting Information Fig. 3 was used for the DW-ML characterization measurements. A collimated beam was used to illuminate the DW-ML and the intensity distribution was imaged at multiple planes around the focal plane and parallel to it. These images were compiled to form the axial intensity distribution profiles of **Figure 3**b and **Figure 3**c. The two-photon image in **Figure 4**b is captured by replacing the objective lens in a two-photon microscope by the DW-ML. The DW-ML was oriented in such a way that the excitation axis of the metasurface (corresponding to the 820-nm wavelength) overlapped with the polarization direction of the excitation laser. The details of the two-photon microscope are shown in Supporting Information Fig. 1. A photomultiplier tube is used for detection of the emitted photons, and the image is captured by scanning the excitation focal spot of the lens using the

galvanometer scanning mirror. The final image is then generated by combining the collected signal for each excitation point. Using this method, the field of view of the microscope is limited by two different factors: first, the available angular scanning range of the excitation optics, and second, the off-axis aberrations of the meta-lens. In our case, the large off-axis aberrations of the meta-lens[31] limit the field of view to about $\pm 2.5^{\circ}$, which corresponds to about 120 μm. Both the DW-ML and the refractive objective are used to image a polyethylene microsphere about 90 μm in diameter and coated with a fluorophore (UVPMS-BR-0.995 10-90m μm, Cospheric). This specific fluorophore was chosen because its excitation and emission wavelengths are compatible with the p-Si material system, and the birefringent meta-atom strategy used to design the DW-ML. In addition, the specific fluorophore-coated microspheres were used because they are commercially available samples coated with the right fluorophores.

Acknowledgement

This work was supported by National Science Foundation award 1512266. Dr. Jiaqi Li gratefully acknowledges the financial support from FWO (Flanders). We sgratefully acknowledge critical support and infrastructure provided for this work by the Kavli Nanoscience Institute at Caltech. The two-photon microscope was designed and built at the Caltech Neurotechnology Center with support from the Beckman Institute. The authors would like to thank the helpful discussions with Dr. Alon Greenbaum, Dr. Min Jee Jang, and Sripriya Kumar.

Notes. The authors declare no competing financial interest.

Supporting Information. Supporting Information Figs. 1 to 3 include the details of the two-photon microscope, extended simulation results, and measurement setups. Supporting Information Section 1 includes notes on the focusing efficiency of the DW-ML for a signal with a considerable bandwidth.

References

(1) Denk, W.; Strickler, J.; Webb, W. *Science* **1990**, *248*, 73–76.

(2) Konig, K. *Jour. Microsc.* **2000**, *200*, 83–104.

(3) Zipfel, W. R.; Williams, R. M.; Webb, W. W. *Nat. Biotechnol.* **2003**, *21*, 1369–1377.

(4) Helmchen, F.; Denk, W. *Nat. Methods* **2005**, *2*, 932–940.

(5) Helmchen, F.; Fee, M. S.; Tank, D. W.; Denk, W. *Neuron* **2001**, *31*, 903–912.

(6) Konig, K.; Ehlers, A.; Riemann, I.; Schenkl, S.; Buckle, R.; Kaatz, M. *Microsc. Res. Tech.* **2007**, *70*, 398–402.

(7) Engelbrecht, C. J.; Johnston, R. S.; Seibel, E. J.; Helmchen, F. *Opt. Express* **2008**, *16*, 5556–5564.

(8) Hoy, C. L.; Durr, N. J.; Chen, P.; Piyawattanametha, W.; Ra, H.; Solgaard, O.; Ben-Yakar, A. *Opt. Express* **2008**, *16*, 9996–10005.

(9) Piyawattanametha, W.; Cocker, E. D.; Burns, L. D.; Barretto, R. P. J.; Jung, J. C.; Ra, H.; Solgaard, O.; Schnitzer, M. J. *Opt. Lett.* **2009**, *34*, 2309–2311.

(10) Zong, W.; Wu, R.; Li, M.; Hu, Y.; Li, Y.; Li, J.; Rong, H.; Wu, H.; Xu, Y.; Lu, Y. e. a. *Nat. Methods* **2017**, *14*, 713–719.

(11) Hsiao, H.-H.; Chu, C. H.; Tsai, D. P. *Small Methods* **2017**, *1*, 1600064.

(12) Kruk, S.; Kivshar, Y. *ACS Photonics* **2017**, *4*, 2638–2649.

(13) Kamali, S. M.; Arbabi, E.; Arbabi, A.; Faraon, A. *Nanophotonics* **2018**, *7*, 1041–1068.

(14) Lalanne, P.; Astilean, S.; Chavel, P.; Cambril, E.; Launois, H. *Opt. Lett.* **1998**, *23*, 1081–1083.

(15) Arbabi, A.; Horie, Y.; Ball, A. J.; Bagheri, M.; Faraon, A. *Nat. Commun.* **2015**, *6*, 7069.

(16) Khorasaninejad, M.; Chen, W. T.; Devlin, R. C.; Oh, J.; Zhu, A. Y.; Capasso, F. *Science* **2016**, *352*, 1190–1194.

(17) Colburn, S.; Zhan, A.; Majumdar, A. *Sci. Adv.* **2018**, *4*, eaar2114.

(18) Paniagua-Dominguez, R.; Yu, Y.; Khaidarov, E.; Choi, S.; Leong, V.; Bakker, R. M.; Liang, X.; Fu, Y. H.; Valuckas, V.; Krivitsky, L. A. e. a. *Nano Lett.* **2018**, *18*, 2124–2132.

(19) Kamali, S. M.; Arbabi, E.; Arbabi, A.; Horie, Y.; Faraon, A. *Laser Photon. Rev.* **2016**, *10*, 1062–1062.

(20) She, A.; Zhang, S.; Shian, S.; Clarke, D. R.; Capasso, F. *Sci. Adv.* **2018**, *4*, eaap9957.

(21) Arbabi, E.; Arbabi, A.; Kamali, S. M.; Horie, Y.; Faraji-Dana, M.; Faraon, A. *Nat. Commun.* **2018**, *9*, 812.

(22) Arbabi, A.; Horie, Y.; Bagheri, M.; Faraon, A. *Nat. Nanotechnol.* **2015**, *10*, 937–943.

(23) Maguid, E.; Yannai, M.; Faerman, A.; Yulevich, I.; Kleiner, V.; Hasman, E. *Science* **2017**, *358*, 1411–1415.

(24) Li, J.; Verellen, N.; Vercruysse, D.; Bearda, T.; Lagae, L.; Van Dorpe, P. *Nano Lett.* **2016**, *16*, 4396–4403.

(25) Rahmani, M.; Xu, L.; Miroshnichenko, A. E.; Komar, A.; Camacho-Morales, R.; Chen, H.; Zrate, Y.; Kruk, S.; Zhang, G.; Neshev, D. N. e. a. *Adv. Funct. Mater.* **2017**, *27*, 1700580.

(26) Kamali, S. M.; Arbabi, A.; Arbabi, E.; Horie, Y.; Faraon, A. *Nat. Commun.* **2016**, *7*, 11618.

(27) Yin, X.; Steinle, T.; Huang, L.; Taubner, T.; Wuttig, M.; Zentgraf, T.; Giessen, H. *Light: Sci. Appl.* **2017**, *6*, e17016.

(28) Schlickriede, C.; Waterman, N.; Reineke, B.; Georgi, P.; Li, G.; Zhang, S.; Zentgraf, T. *Adv. Mater.* **2018**, *30*, 1703843.

(29) Kamali, S. M.; Arbabi, E.; Arbabi, A.; Horie, Y.; Faraji-Dana, M.; Faraon, A. *Phys. Rev. X* **2017**, *7*, 041056.

(30) Emani, N. K.; Khaidarov, E.; Paniagua-Dominguez, R.; Fu, Y. H.; Valuckas, V.; Lu, S.; Zhang, X.; Tan, S. T.; Demir, H. V.; Kuznetsov, A. I. *Appl. Phys. Lett.* **2017**, *111*, 221101.

(31) Arbabi, A.; Arbabi, E.; Kamali, S. M.; Horie, Y.; Han, S.; Faraon, A. *Nat. Commun.* **2016**, *7*, 13682.

(32) Miyamoto, K. *J. Opt. Soc. Am.* **1961**, *51*, 17–20.

(33) Born, M.; Wolf, E. *Principles of Optics: Electromagnetic Theory of Propagation, Interference and Diffraction of Light*; Cambridge University Press, 1999.

(34) O'Shea, D. C.; Suleski, T. J.; Kathman, A. D.; Prather, D. W. *Diffractive Optics: Design, Fabrication, and Test*; SPIE Press, 2004.

(35) Arbabi, E.; Arbabi, A.; Kamali, S. M.; Horie, Y.; Faraon, A. *Optica* **2017**, *4*, 625–632.

(36) Arbabi, E.; Arbabi, A.; Kamali, S. M.; Horie, Y.; Faraon, A. *Opt. Express* **2016**, *24*, 18468–18477.

(37) Wang, S.; Wu, P. C.; Su, V.-C.; Lai, Y.-C.; Chen, M.-K.; Kuo, H. Y.; Chen, B. H.; Chen, Y. H.; Huang, T.-T.; Wang, J.-H. e. a. *Nat. Nanotechnol.* **2018**, *13*, 227–232.

(38) Sell, D.; Yang, J.; Doshay, S.; Fan, J. A. *Adv. Opt. Mater.* **2017**, *5*, 1700645.

(39) Zhan, A.; Colburn, S.; Dodson, C. M.; Majumdar, A. *Sci. Rep.* **2017**, *7*, 1673.

(40) Groever, B.; Chen, W. T.; Capasso, F. *Nano Lett.* **2017**, *17*, 4902–4907.

(41) Arbabi, E.; Arbabi, A.; Kamali, S. M.; Horie, Y.; Faraon, A. *Optica* **2016**, *3*, 628–633.

(42) Wang, B.; Dong, F.; Yang, D.; Song, Z.; Xu, L.; Chu, W.; Gong, Q.; Li, Y. *Optica* **2017**, *4*, 1368–1371.

(43) Lin, D.; Holsteen, A. L.; Maguid, E.; Wetzstein, G.; Kik, P. G.; Hasman, E.; Brongersma, M. L. *Nano Lett.* **2016**, *16*, 7671–7676.

(44) Arbabi, E.; Arbabi, A.; Kamali, S. M.; Horie, Y.; Faraon, A. *Sci. Rep.* **2016**, *6*, 32803.

(45) Makarov, S. V.; Petrov, M. I.; Zywietz, U.; Milichko, V.; Zuev, D.; Lopanitsyna, N.; Kuksin, A.; Mukhin, I.; Zograf, G.; Ubyivovk, E. e. a. *Nano Lett.* **2017**, *17*, 3047–3053.

(46) Liu, V.; Fan, S. *Comput. Phys. Commun.* **2012**, *183*, 2233–2244.

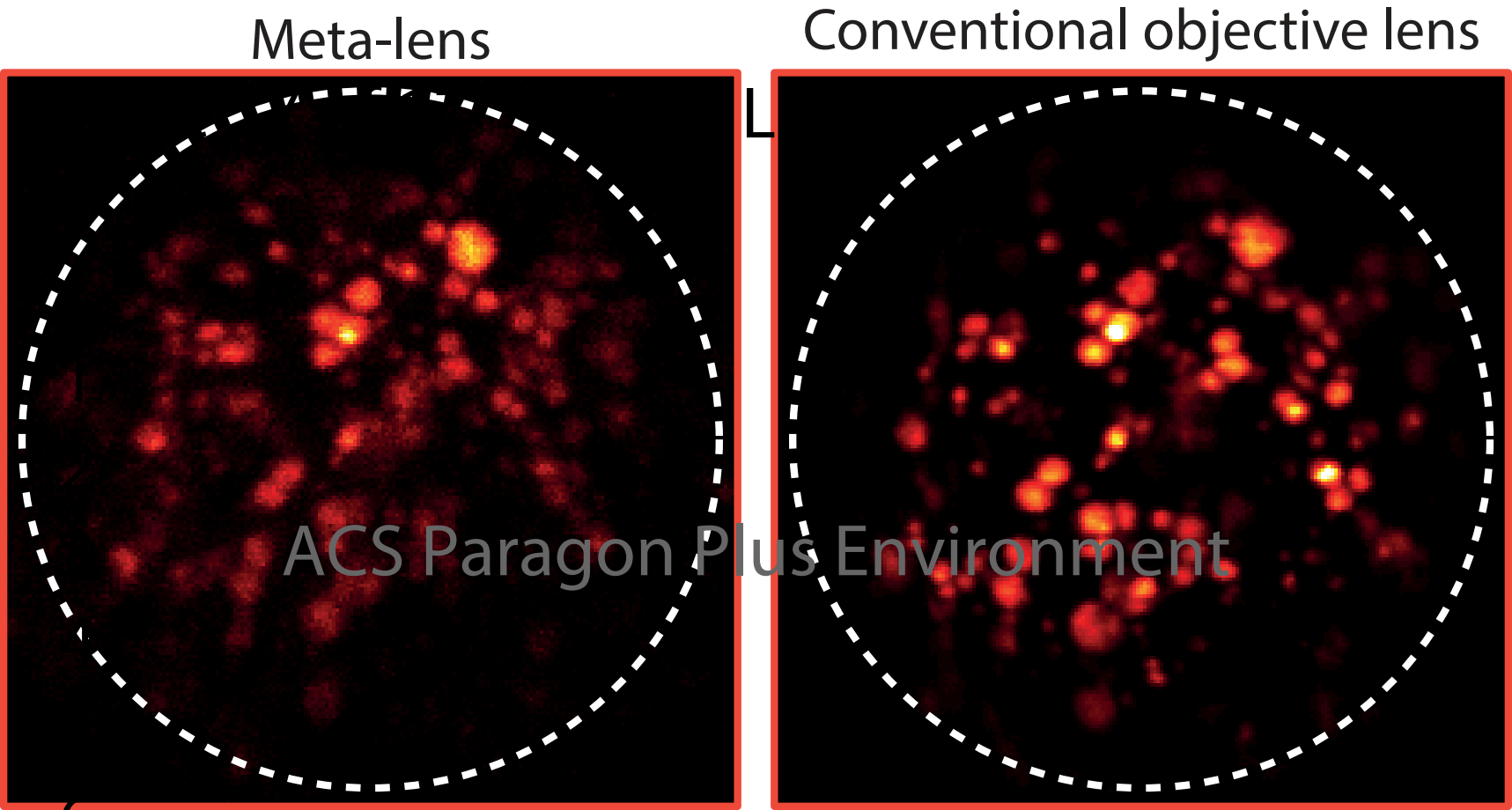
Meta-lens
Conventional objective lens
ACS Paragon Plus Environment